Incorporating Electron Range Approximations into Secondary Electron Emission Models

Gregory Wilson

***Abstract*—Secondary Electron Yield is a key parameter in spacecraft charging. In order to develop a robust model to predict the secondary electron yield for any given material, the work done by Utah State University's Materials Physics Group on electron range is extended to the yield problem. This newly developed yield model uses the probabilistic nature of inelastic collisions to incorporate the material dependent inelastic mean free path model used in USU's MPG's range model.**

***Keywords*—Electron emission, electron range, penetration depth, energetic electron bombardment, multilayer materials**

I. Introduction

Spacecraft charging is the leading cause of spacecraft failure due to the space environment. In order to mitigate deleterious charging phenomenon, an understanding of material interaction with the space environment is essential. One of the driving phenomenons of spacecraft charging is secondary electron emission (SEE). SEE has been studied extensively for spacecraft charging as well as for electron spectroscopy.

Several semi-empirical models have been developed in order to fit SEE data. However, due to the uncertainty in the stopping power, inelastic mean free path, and the electron range at low energies (∼50 eV), predictive models have been far more difficult to develop. This paper describes an attempt to use the electron range models developed by Utah State University's (USU) Materials Physics Group (MPG) to create a predictive model for the secondary electron yield (SEY). The development of one of the most general methods will be described which will lead into the development of a predictive model based on USU's MPG's work on electron range.

II. Electron Range

The range, R, or maximum distance an electron of a given incident energy can penetrate through a material before all kinetic energy is dissipated and the electron comes to rest, is a common way to parameterize electron interactions with materials. The range differs from the penetration depth which is the distance a material penetrates as measured from the surface whereas the range is a measure of the total path length of the electron since it ignores all elastic collisions and deviations in trajectory.

The range is often used in spacecraft charging calculations to predict the charge distribution of deposited electrons in materials as well as the modeling of secondary and backscattered electron emission. It is also used to predict the distribution of energy deposited by incident electrons as they traverse a material [1], [2]; this distribution is further used to model radiation induced conductivity and cathodoluminescence.

Gregory Wilson is with the Materials Physics Group in the Physics Department at Utah State University in Logan, UT 84322 USA (e-mail: gregdwilson@gmail.com)

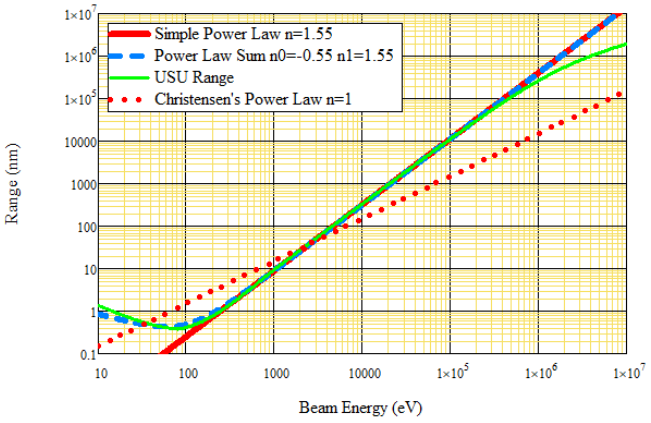

Fig. 1. Electron range versus incident beam energy for the various electron range models for Au. The Simple Power Law Model uses Eq. 1 with an exponent of 1.55 and a factor of b set to fit the NIST ESTAR database. The power law sum uses Eq. 2 with exponents -0.55 and 1.55 for n_0 and n_1 respectively with values of b_1 and b_2 set to fit the model to data. The USU Range use Eq. 3 with N_v set to fit the NIST Data. The Christensen Power Law model is a simple power law using Eq. 1 with b and n set so that the yield model with $m = 0.6$ matches the yield data as shown in Fig. 7b.

The primary energy loss mechanism for electrons is due to inelastic collisions within material. This is generally split into two categories, plasmon-pole excitations and single-electron excitations [3]. Due to the probabilistic nature of this mechanism, the Continuous Slow Down Approximation (CSDA) is often employed to simplify the problem. In the CSDA, the rate of energy loss, dE/dz (termed the total stopping power) is assumed equal to the total stopping power at every position along the penetration path; variations in energy-loss rate with energy, E, or with penetration depth, z, are neglected.

Detailed expressions for the range have been developed starting from early work by Bethe [4]; however, these models often have restricted energy ranges of applicability and involve many fitting parameters. One of the most common approximations is given by:

$$R(E) = bE^n \tag{1}$$

where the value of n is a constant between 1 and 2 [5]–[8].

A more general form used in the NASCAP charging code [9] is given by the summation of two power laws [10] of the form,

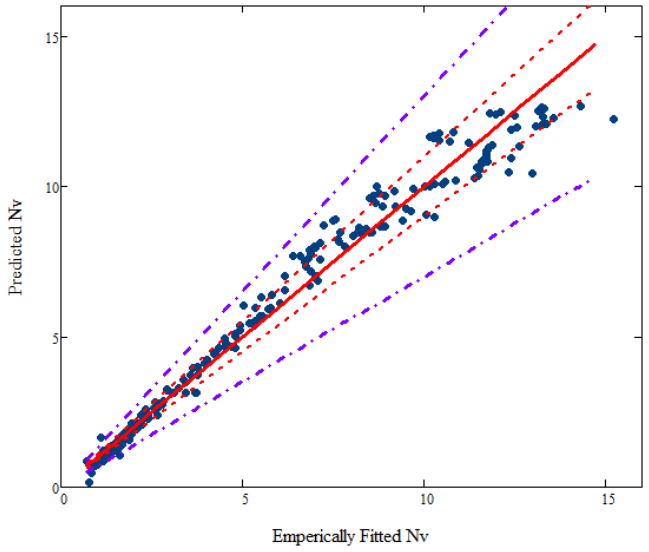

Fig. 2. Comparison of predicted N_v^{pre} values to empirical N_v^{eff} values. The red and purple dashed lines represent 10% and 30% deviations, respectively, from an exact one-to-one linear fit (solid red).

$$R(E) = b_1 E^{n_1} + b_2 E^{n_2} \tag{2}$$

Using the CSDA as well as a Constant Loss Approximation (CLA) [11] for high energies and an extension of the innelastic mean free path for low energies, the MPG at USU has developed a composite analytic approximation to the range, spanning incident energies from <10 eV to >100 MeV, with a single fitting parameter, N_v^{eff}, that can be readily implemented for a wide array of conducting, semiconducting and insulating spacecraft materials [12], [13]. This formula is given as:

$$R\left(E_b; N_v^{eff}\right) = \begin{cases} \left[\frac{E_b}{\bar{E}}\right] \lambda_{\text{IMFP}}\left(\bar{E}\right) \left(\frac{1-e^{-\bar{E}/\bar{E}}}{1-e^{-E_b/\bar{E}}}\right)^2 & \text{if } E_b < \bar{E} \\ \left[\frac{E_b}{\bar{E}}\right] \lambda_{\text{IMFP}}\left(E_b\right) \left(\frac{1-e^{-\bar{E}/\bar{E}}}{1-e^{-E_b/\bar{E}}}\right) & \text{if } \bar{E} \le E_b \le E_{\text{HI}} \\ b\, E_b^n \left[1 - \left[1 + \left(\frac{E_b/N_v^{eff}}{m_e\, c^2}\right)\right]^{-2}\right] & \text{if } E_b > E_{\text{HI}} \end{cases} \tag{3}$$

where the inelastic mean free path, $\lambda_{IMFP}(E)$ is given by the TPP-2M formula [14] fit to the NIST IMFP database [15] where data is available:

$$\lambda_{IMFP}(E) = E\left[E_p^{eff}\right]^{-2}\left[\beta \ln\left(\gamma E\right) - CE^{-1} + DE^{-2}\right]^{-1} \tag{4}$$

where β, γ, C, and D are defined in [14] and n and b are defined by [12]. In order to make this formula a predictive model, a predictive formula for N_v^{eff} was developed.

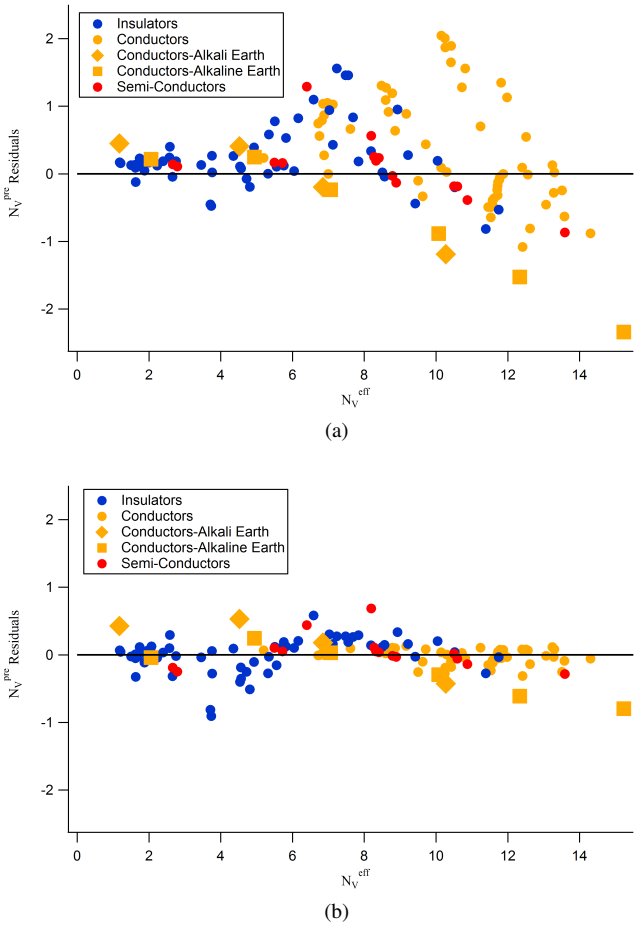

Fig. 3. Residuals (N_v^{pre} - N_v^{eff}) versus empirical N_v^{eff} values. The different symbols indicate different material types. (a): Without the density correction: (b): With the density correction.

Originally, N_v^{eff} were empirically determined by fitting the model to the ESTAR and IMFP NIST databases [15]. These values were then compared to several material properties. Using a least squares regression method, a predictive formula for N_v^{pre} was developed, given by:

$$N_v^{pre}(\bar{Z}_A, \rho_m) = N_0\left(\bar{Z}_A^{n_0} + N_{offset}\right) - N_1\left(\rho_m - n_1 \bar{Z}_A\right) \tag{5}$$

where $\bar{Z}_A$ is the mean atomic number weighted by atomic fraction which can be easily determined from the stoichiometric formula for compounds or from elemental fractions for composite materials as

$$\bar{Z}_A \equiv \frac{\left[\sum_i f_i Z_{Ai}\right]}{\left[\sum_i f_i\right]} \tag{6}$$

Although the linear fit of N_v^{pre} vs N_v^{eff} as shown in Fig. 2 showed reasonable agreement, they exhibited a clear pattern which is even more evident when categorized into material type as shown in the residuals depicted in Fig. 3a. The observed patterns were very reminiscent of the deviations

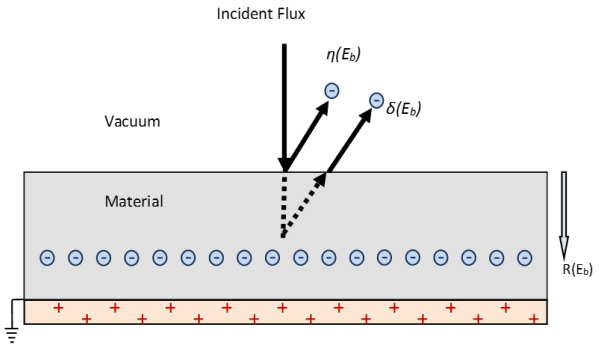

Fig. 4. Diagram of incident electron flux impinging on a generic material. $\eta(E_b)$ denotes the backscattered yield for electrons that originate within the incident beam or that have emission energies E>50 eV. $\delta(E_b)$ denotes the secondary yield for electrons liberated from within the material or that have emission energies E<50 eV. The total yield for all emission energies is the sum of the secondary and backscattered yield; $\sigma(E_b) = \eta(E_b) + \delta(E_b)$. $R(E_b)$ is the incident energy-dependent electron range [1], [12].

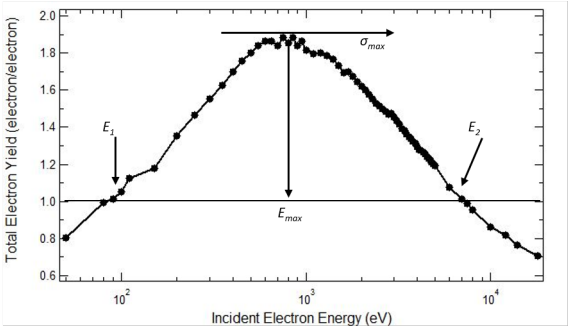

Fig. 5. Total electron yield of polycrystalline Au as a function of incident energy. Data were taken using a DC electron beam. E_1 and E_2 are the first and second crossover energies where yield with $\sigma > 1$ occur when $E_1 < E_b < E_2$. The yield peak, σ_{max}, is the maximum yield and occurs between the crossover energies at E_{max}. (Hoffmann, 2010)

from linearity seen in plots of density versus atomic number for the elements [16].

Therefore, a density correction was added as is shown in Eq. 5 with the resulting residuals shown in Fig. 3b. This allowed the range to be predicted for any given material using readily available material properties with reasonable accuracy.

III. Electron Yield

As energetic electrons interact with the surface of materials, they impart energy throughout the material, as described by the range process. If the energy exchange is near the surface, electrons in the material can be excited and emitted. It is also possible for the incident electron to undergo a quasi-elastic collision near the surface, wherein the electron is backscattered from the surface and therefore imparts no charge to the material.

This process of electron emission from the surface, known as the electron yield, is highly dependent upon the incident electron energy. The total electron yield, defined as the ratio of emitted to incident flux is fundamental in understanding the charging of materials [1].

The incident flux is the total number of electrons entering the material from the environment. The incident flux in a space environment consists of a distribution of energetic electrons at different energies and different incident angles, however, most spacecraft models of secondary emission only consider monoenergetic beams of electrons and then extrapolate to multi-energetic environments.

The emitted flux is the sum of backscattered and secondary electrons, as shown in Fig. 4. Secondary electrons, which originate within the material, conventionally have energies <50 eV where backscattered electrons, which originate from the incident beam, conventionally have energies >50 eV. Secondary yield is then defined as the ratio of secondary electrons to the incident electrons, denoted as $\delta(E_B)$. The backscattered yield is the ratio of backscattered electrons to incident electrons denoted as $\eta(E_b)$ where E_b is the electron beam energy. Thus the total electron yield is the sum of these two, given by $\sigma(E_b) = \eta(E_b) + \delta(E_b)$.

The yield, as shown in Fig. 5, is highly energy dependent with "crossover" energies at E_1 and E_2 and a maximum yield σ_{max} at E_{max}. At very low energies, electrons generally do not have enough energy to excite many electrons, thus low energy electrons generally produce yields less than one. As the energy increases, the probability of multiple collisions near the surface increases which causes the yield to rise above one.

As the energy increases, the electron inelastic mean free path increases causing the collisions to occur deeper within the material, decreasing the likelihood of the electron reaching and then escaping the surface; this leads to a decrease in σ above E_{max}

To model secondary electron emisssion, the general formula is usually given by [7], [17]:

$$\delta(E_b) = \int_0^{R(E_b)} n(z, E_b) P(z) dz \tag{7}$$

where $R(E_b)$ is the range or the maximum depth at which electrons penetrate with a given beam energy E_b, $n(z, E_b)$ is the average number of secondary electrons produced per unit of penetration depth, dz, and P(z) is the probability of the electron reaching and escaping the surface from a depth z.

The differences between different models are most often attributed to variations of assumptions and forms of these functions. The general assumptions that are most commonly used are as follows:

1) One-Dimension - In order to simplify the range, penetration depth and probability of escape, a one dimensional model is used with a normally incident beam and all backscattered electrons are emitted normal to the surface.
2) Mean Field Excitations - Secondary electron production is assumed to be solely dependent on the total stopping power scaled by the mean field energy, ϵ_m, required to

produce a secondary electron given by:

$$n(z, E_b) = -\frac{1}{\epsilon_m}\frac{dE}{dz} \tag{8}$$

3) Range Approximations - The continuous slowdown approximation is often incorporated in order to simplify the range by assuming that the change in energy dE of an electron through a given distance dz is equal to the total stopping power $S(E)$, neglecting energy loss deviations. Note that the energy E in this equation is the current energy of the electron and not the incident energy. This allows the range to be approximated by:

$$R(E_b) = \int_{10eV}^{E_b} \frac{dE}{S(E)} \tag{9}$$

which is known as the CSDA range. The CSDA range can further be approximated by power law expressions as explained in Section II.
A more restrictive assumption is the use of the CLA where the stopping power is assumed constant and equal to the average stopping power over the entire path length of the electron. This allows the relation,

$$\frac{dE}{dz} = -\frac{E_b}{R(E_b)}. \tag{10}$$

This simplifies the mean field excitation approximation by removing any z or energy dependence on the stopping power.

4) Probability of Emission - The probability of secondary electrons leaving the material is dependent on two different phenomena. The first phenemona involves traversing the material and reaching the service from a depth z. The second phenemona involves overcoming the surface barrier and escaping from the material.
The first phenomena is generally approximated by applying the inelastic mean free path of an electron where the probability of traversing a distance z without an inelastic collision is given $e^{-z/\lambda_{SE}}$. In order to account for the direction of emission, a constant factor α is multiplied to this probability. For one dimension, its generally taken as $1/2$.
The second phenomenon involves the probability, β, that an electron will escape the surface which is dependent upon the surface potential along with the electron affinity and band gap of the material [11].
Together, these give a formula of the form:

$$P(z) = \alpha\beta e^{-\frac{z}{\lambda_{SE}}} \tag{11}$$

Putting all of these assumptions together and combining α and β, this gives for the secondary electron yield,

$$\delta(E_b) = \frac{\beta}{2\epsilon_m}\frac{E_b}{R(E_b)}\int_0^{R(E_b)} e^{-\frac{z}{\lambda_{SE}}}\,dz \tag{12}$$

$$= \frac{\beta\lambda_{SE}}{2R(E_b)}\frac{E_b}{\epsilon_m}\left(1 - e^{-\frac{R(E_b)}{\lambda_{SE}}}\right) \tag{13}$$

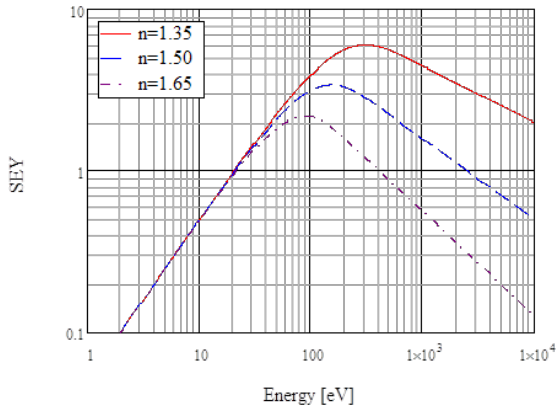

Fig. 6. A model for the secondary electron yield using a simple power law model for the range as shown in Eq. 14 with varying powers of n in the range model. Markers for the first and second cross over energies are given by E_1 and E_2 respectively. The maximum yield δ_{max} at E_{max} are also indicated. Note that increasing n shifts E_{max} to the left and δ_{max} down.

If a power law range is assumed as given by Eq. 1 then the equation becomes

$$\delta(E_b) = \frac{\beta\lambda_{SE}}{2b\epsilon_m}E_b^{1-n}\left(1 - e^{-\frac{bE_b^n}{\lambda_{SE}}}\right) \tag{14}$$

Figure 6 shows this model for the yield using different values of n in the range approximation.

IV. Predictive Yield Modeling

The easiest way to incorporate the range into the secondary yield model is to plug Eq. 3 into Eq. 13. The IMFP for secondary electrons can then predicted using the TPP-2M equation using the same parameters used in the range equation. That leaves β, ϵ_m, and E_{SE}, the average kinetic energy of the secondary electrons used to determine the IMFP.

These parameters can be approximated using the assumptions in Section II along with the general assumption that the mean secondary electron energy as given by [19]. Figure 7a shows the models of secondary electron emission as a function incident beam energy using Eq. 13 using the different models of the range. As is seen, the differences in the range are slight and only become apparent at low energies.

This graph highlights one of the issues with the yield model itself, which often has difficulty fitting the data at low energies. In order to make a better fit, Christensen developed a model [18] similar to the Sternglass model [20], with a varying parameter, m, which changes the slope of the yield at low energies as shown in Fig. 7b.

While this creates a better fit for the yield, the resulting parameters, when plugged back into the range model used, give an unrealistic version of the range as shown in Fig. 7. When this power of m is introduced into the yield models using the other approximations for the range, it gives a better fit at low energies, but causes the slope at high energies to be too steep. Thus, in order to use this extra fitting parameter m

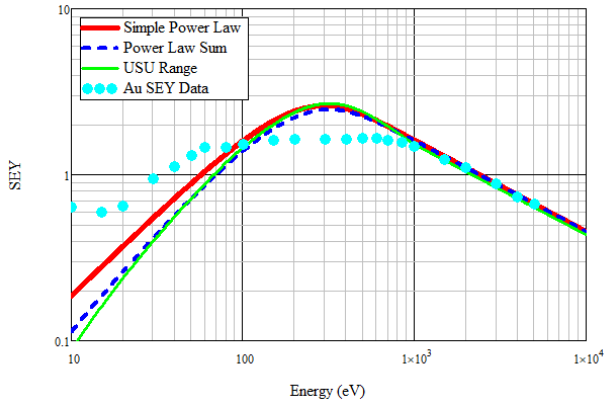

(a)

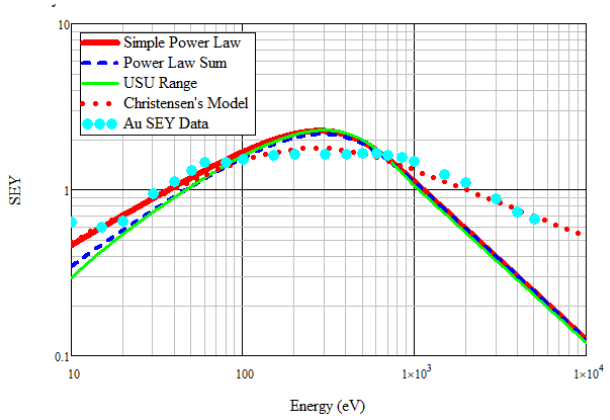

(b)

Fig. 7. Graphs of the various secondary electron yield models for Au vs the incident electron energy along with Au SEY data taken by USU's MPG. (a) Using the models as discussed in this paper. (b) Using an extra product of E^m as discussed in [18]

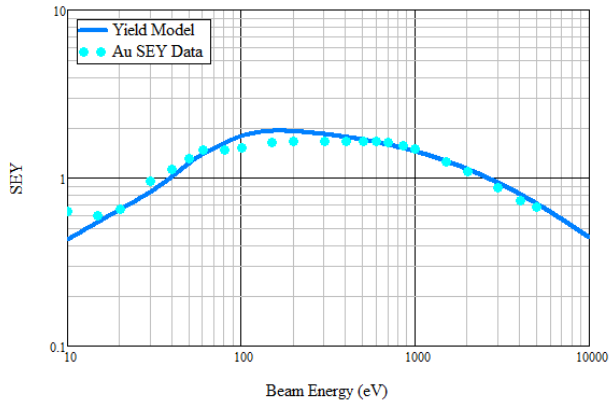

(a) Au

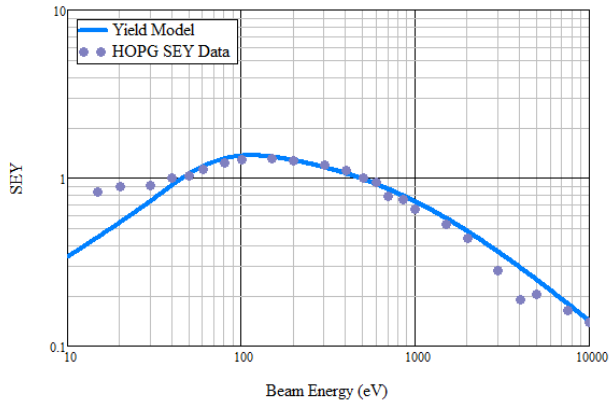

(b) HOPG

Fig. 8. A model for the secondary electron yield using a probabilistic model based on the IMFP using parameters determined by USU's MPG electron range model and using $\epsilon_m = 4eV$, $\sigma = 10eV$ and (a) $E_{SE} = 3eV$ and $\beta = 0.85$ for Au (b) $E_{SE} = 4eV$ and $\beta = 0.7$ for HOPG.

with accurate approximations for the range, a better physical representation of m must be developed.

To approach the problem from another angle, the calculations for the IMFP used in the range approximation were used to develop a different function for $n(z, E_b)$ given by

$$n(z, E_b) = \sum_i \left(P_i^{coll}(z, E_b) P_i^{exct}(E_b) \right) \tag{15}$$

where $P_i^{coll}(z, E)$ is the probability of an i'th collision at a depth z and $P_i^{exct}(E)$ is the probability of a collision producing a secondary electron from a primary electron with energy E.

Using, the IMFP, the probability density of the i'th collision occurring in a given dz can be approximated by the Gamma distribution given by

$$P_i^{coll}(z, E_b) = \frac{1}{\Gamma(i)\lambda(E_b)^i} z^{i-1} e^{-\frac{z}{\lambda(E_b)}} \tag{16}$$

The probability of a secondary electron being generated can be approximated by the Fermi-Dirac probability distribution function giving the form:

$$P_i^{exct}(E_b) = \frac{1}{1 + e^{-\frac{(E_b - (i-1)\bar{E}) - \epsilon_m}{\sigma}}} \tag{17}$$

where $(i-1)\bar{E}$ is the energy lost in the previous $(i-1)$ collisions where $\bar{E}$ is the mean energy lost per collision as defined by the range.

Multiplying Eq. 15 by Eq. 11 and integrating over all z as in Eq. 7 and combining β and α in Eq. 11 gives

$$\delta(E_b) = \sum_i \left(\frac{\lambda_{SE}}{(\lambda_{SE} + \lambda(E_b))} \right)^i \frac{\beta}{(i-1)!} \frac{1}{1 + e^{-\frac{(E_b - (i-1)\bar{E}) - \epsilon_m}{\sigma}}} \tag{18}$$

where the fitting parameters are the energy of secondary electrons E_{SE} which determines λ_{SE}, the energy required to excite an electron given by ϵ_m and distribution of states from which electrons can be excited given by σ.

E_{SE} changes the slopes at both high and low energies and shifts the graph vertically. Changing ϵ_m primarily changes the

slope at low energies and σ effects the discrete nature of the number of collisions resulting in steps at low energies for small values of σ. It was shown that the first three terms in the sum were significant with changes in the yield above five collisions becoming negligible.

V. Conclusion

Secondary electron yield models are varied both in form and in complexity. While complex models such as those developed using the Full Penn Algorithm [21] or those employing Monte Carlo methods can produce models that fit extremely well to data [22], these models are difficult to employ and nearly impossible to use in a predictive method.

To approach the problem with simpler and more straightforward methods can produce the opposite result where no amount of tweaking of the parameters can fit the model to the data.

USU's MPG model of the electron range is an example of merging both worlds by creating an easy to use model that functions over a wide energy range for a substantial number of elements. Coupled with the ability to predict ranges for complex materials with a minimal number of well defined material parameters this tool becomes a perfect base to build other useful tools.

Building upon the backbone of this model, a robust yield model has now begun to be developed with the potential of predicting the yield of hundreds of materials already in the database and potentially limitless more using the predictive capabilities already developed in the range model.

Further testing, tweaking and validating must be done in order to verify that not only does the model fit a plethora of data, but that the physical models used will remain valid when the fitting parameters are tweaked to fit those data. The model can also be adjusted to incorporate a three-dimensional model of secondary electron excitation, traversal and emission as was done for the simple power law model by Christensen [18] or any other more refined adjustments that will improve the model while still keeping the needed inputs to a minimum.

References

[1] R. Hoffmann, "Electron-induced electron yields of uncharged insulating materials," Master's thesis, Utah State University, Logan, UT, 2010.

[2] C. Thomson, "Measurements of the secondary electron emission properties of insulators," PhD Dissertation, Utah State University, Logan, UT, March 2004 2004.

[3] H. Shinotsuka, S. Tanuma, C. J. Powell, and D. R. Penn, "Calculations of electron inelastic mean free paths. x. data for 41 elemental solids over the 50ev to 200kev range with the relativistic full penn algorithm," *Surface and Interface Analysis*, vol. 47, no. 9, pp. 871–888. [Online]. Available: https://onlinelibrary.wiley.com/doi/abs/10.1002/sia.5789

[4] H. Bethe and W. Heitler, "On the stopping of fast particles and on the creation of positive electrons," *Proceedings of the Royal Society of London. Series A, Containing Papers of a Mathematical and Physical Character*, vol. 146, no. 856, pp. 83–112, 1934.

[5] J. Young, "Penetration of electrons and ions in aluminum," *Journal of Applied Physics*, vol. 27, p. 1, 1956.

[6] R. O. Lane and D. J. Zaffarano, "Transmission of 0-40 kev electrons by thin films with application to beta-ray spectroscopy," *Phys. Rev.*, vol. 94, pp. 960–964, May 1954. [Online]. Available: https://link.aps.org/doi/10.1103/PhysRev.94.960

[7] H. Seiler, "Secondary electron emission in the scanning electron microscope," *Journal of Applied Physics*, vol. 54, no. 11, pp. R1–R18, 1983.

[8] Whiddington, "The transmission of cathode rays through matter," *Royal Society of London. Series A, Containing Papers of a MAthematical and Physical Character*, vol. 89, no. 554, 1914.

[9] M. Mandell, D. Cooke, V. Davis, G. Jongeward, B. Gardner, R. Hilmer, K. Ray, S. Lai, and L. Krause, "Modeling the charging of geosynchronous and interplanetary spacecraft using nascap-2k," *Advances in Space Research*, vol. 36, no. 12, pp. 2511–2515, 2005.

[10] I. Katz, D. E. Parks, M. J. Mandell, J. M. Harvey, S. S. Wang, and J. C. Roche, "Nascap, a three-dimensional charging analyzer program for complex spacecraft," *IEEE Transactions on Nuclear Science*, vol. 24, no. 6, pp. 2276–2280, 1977.

[11] R. Alig and S. Bloom, "Secondary electron escape probabilities," *Journal of Applied Physics*, vol. 49, p. 3476, 1978.

[12] G. Wilson and J. R. Dennison, "Approximation of range in materials as a function of incident electron energy," *IEEE Trans. on Plasma Sci.*, vol. 40, no. 2, pp. 305–310, 2012.

[13] A. Starley, G. Wilson, L. Phillipps, and J. Dennison, "Predictive formula for electron penetration depth of diverse materials over large energy ranges," in *14th Spacecraft Charging Technology Conference*, 2016, Conference Proceedings.

[14] S. Tanuma, C. J. Powell, and D. R. Penn, "Calculations of electron inelastic mean free paths (imfp's) vi. analysis of the gries inelastic scattering model and predictive imfp equation," *Sur. Inter. Anal.*, vol. 25, no. 25, 1997.

[15] N. I. o. S. a. Technology, "Nist electron inelastic-mean-free-path database: Version 1.1," http://www.nist.gov/srd/nist71.htm, 2010.

[16] P. Atkins and S. Mason, "The periodic kingdom: A journey into the land of the chemical elements," *Nature*, vol. 376, no. 6543, pp. 734–734, 1995.

[17] Y. Lin and D. C. Joy, "A new examination of secondary electron yield data," *Surface and interface analysis*, vol. 37, no. 11, pp. 895–900, 2005.

[18] J. Christensen, "Electron yield measurements of high-yield, low-conductivity dielectric materials," Master's thesis, Utah State University, 2017.

[19] M. Chung and T. Everhart, "Simple calculation of energy distribution of low energy secondary electrons emitted from metals under electron bombardment," *Journal of Applied Physics*, vol. 45, p. 707, 1974.

[20] E. Sternglass, "Theory of secondary electron emission by high-speed ions," *Physical Review*, vol. 108, no. 1, p. 1, 1957.

[21] S. F. Mao, Y. G. Li, R. G. Zeng, and Z. J. Ding, "Electron inelastic scattering and secondary electron emission calculated without the single pole approximation," *Journal of Applied Physics*, vol. 104, no. 11, p. 114907, 2008. [Online]. Available: https://doi.org/10.1063/1.3033564

[22] M. A. Furman and M. T. F. Pivi, "Probabilistic model for the simulation of secondary electron emission," *Phys. Rev. ST Accel. Beams*, vol. 5, p. 124404, Dec 2002. [Online]. Available: https://link.aps.org/doi/10.1103/PhysRevSTAB.5.124404

Gregory Wilson received dual B.S. degrees in physics and mathematics from Utah State University in Logan, UT in 2012. He received an MS in physics from Montana State University in Bozeman, MT in 2015. He is currently a PhD student in physics at Utah State University. He has worked with the Materials Physics Group for four years on electron emission and luminescence studies related to spacecraft charging.